

## Plane-polarized Raman continuum in the insulating and superconducting layered cuprates

D. Reznik,\* S. L. Cooper, M. V. Klein, W. C. Lee, and D. M. Ginsberg

*Department of Physics and Science and Technology Center for Superconductivity, University of Illinois, Urbana, Illinois 81801*

A. A. Maksimov, A. V. Puchkov,<sup>†</sup> and I. I. Tartakovskii

*Institute of Solid State Physics, Russian Academy of Sciences, 142432, Chernogolovka, Moscow Oblast, Russia*

S-W. Cheong

*AT&T Bell Laboratories, Murray Hill, New Jersey 07974*

(Received 8 February 1993; revised manuscript received 3 May 1993)

Electronic properties of copper oxygen planes (and chains in Y-Ba-Cu-O) were studied with Raman spectroscopy of plane-polarized photons. The electronic continuum was found to be independent of doping in 2:1:4 and 1:2:3 materials at energies above  $\sim 1000 \text{ cm}^{-1}$ . Temperature dependence at low energies differs significantly in undoped, lightly doped, and fully doped  $\text{YBa}_2\text{Cu}_3\text{O}_{6+x}$ . A feature consistent with the *superconducting gap* was observed below  $T_c$  in  $\text{YBa}_2\text{Cu}_3\text{O}_{6.9}$  in all scattering geometries. However, the gaplike redistribution was not complete, with 40–60% of states not shifted to higher energies at temperatures well below  $T_c$ . Above  $T_c$  the temperature dependence strongly depends on scattering geometry: the continuum is *temperature independent* (marginal-Fermi-liquid-like) in  $XX$  ( $x^2$ ) and  $X'X'$  ( $x^2+y^2$ ) geometry; it has a *Bose-factor temperature dependence* in  $X'Y'$  ( $x^2-y^2$ ) geometry, and a weak temperature dependence somewhat smaller than the Bose factor in  $YY$  ( $y^2$ ) geometry. A *two-boson-like* temperature dependence of the low-energy continuum is found in  $\text{YBa}_2\text{Cu}_3\text{O}_{6.1}$  and  $\text{Sm}_2\text{CuO}_4$ . It becomes one-particle-like in Y-Ba-Cu-O once small doping levels are introduced. Constraints these results place on theoretical models are discussed.

### I. INTRODUCTION

By now it is well known that Raman spectra of copper oxide superconductors are dominated by a broad continuum. It was shown in Ref. 1 that the microscopic origins of the continuum scattering differ for  $c$ -axis- and plane-polarized photons. The  $c$ -axis-polarized continuum is discussed in detail in Ref. 2. The present paper presents the results of a detailed study of the doping, polarization, laser frequency, and temperature dependence of the plane-polarized continuum and two-magnon scattering in  $\text{YBa}_2\text{Cu}_3\text{O}_{6+\delta}$  (YBCO) and  $\text{Sm}_2\text{CuO}_4$  and compares these results as well as results obtained by other groups to theoretical predictions.

### II. EXPERIMENTAL

#### A. Setup

Data shown in Figs. 3, 4, 8, 13, and 15–17 were taken on a Spex “Triplemate” Raman spectrometer with a CCD detector. The sample was in a flowing helium cryostat. A 12 mW laser beam was focused on the sample to a spot of  $\sim 50 \times 50 \mu\text{m}$  for Figs. 3, 4, and 8, and  $\sim 100 \times 200 \mu\text{m}$  for Figs. 13 and 15–17. Raman spectra of YBCO single crystals in  $XX$ ,  $YY$ ,  $XY$ , and  $YX$  scattering geometries were taken from  $ab$  faces of untwinned and twinned  $\text{YBa}_2\text{Cu}_3\text{O}_x$  single crystals. [Notation:  $XY$  means that incident photons are polarized along  $X$ , scattered along  $Y$ ;  $X$  is parallel to the  $a$  axis,  $Y$  is the  $b$  axis

(Cu-O chain in YBCO),  $X'$  is a direction  $45^\circ$  from the  $a$  axis,  $Y'$  is perpendicular to  $X'$ , and  $Z$  is the  $c$  axis.]

Data shown in Figs. 9–12 and 14 were taken on a Dilor  $XY$  Raman spectrometer with a multichannel diode array detector. Laser power in these measurements was 13 mW. Laser spot size was  $\sim 100 \times 500 \mu\text{m}$ , which gives a power density of  $\sim 2 \text{ W/cm}^2$ .

#### B. Samples

The single crystals of  $\text{YBa}_2\text{Cu}_3\text{O}_{7-\delta}$  ( $T_c = 90, 66, \text{ and } 0 \text{ K}$ ) with dimensions of  $\sim 0.05 \times 1 \times 1 \text{ mm}$  were grown by a flux method using yttria stabilized zirconia crucibles.<sup>3</sup> The as-grown crystals are insulating with  $0.65 \ll \delta \ll 0.8$ . The crystals were annealed in flowing oxygen at  $600^\circ\text{C}$  for 1 h, then cooled to  $400^\circ\text{C}$  for another hour, annealed at  $400^\circ\text{C}$  for 4 days, and then rapidly cooled to room temperature. The resulting crystals had transition temperatures of 91 K. Microanalysis of these crystals showed less than 12 ppm of Zr impurities. No other impurities were found.

Untwinned crystals with a transition temperature of 66 K were obtained by annealing the as grown crystals in flowing oxygen at  $650^\circ\text{C}$  for 10 days followed by a fast quenching to liquid-nitrogen temperature. Transition widths of the  $T_c = 90$  and 66 K crystals in the magnetization data are  $\sim 1$  and  $\sim 3 \text{ K}$ , respectively. Stoichiometry of the  $T_c = 66 \text{ K}$  crystals was  $\text{YBa}_2\text{Cu}_3\text{O}_{6.6}$ .

To obtain crystals with lower oxygen content than the as-grown ones, the as grown crystals were annealed in nitrogen for 48 h at  $650^\circ\text{C}$  with a fast quench to 77 K, re-

sulting in the stoichiometry of  $\text{YBa}_2\text{Cu}_3\text{O}_{6.1}$ .

Many different samples grown by the method described above were measured in the Raman scattering experiments. Spectra of all samples which went through the same annealing process were identical.

The preparation procedure of the insulating  $\text{Sm}_2\text{CuO}_4$  crystal used in this study is described elsewhere.<sup>4</sup>

### C. Corrections for optical constants

The Raman scattering power  $P_s$  is equal to

$$P_s = I_L T_i T_s V \Omega_{\text{in}} \Delta\omega \frac{d\sigma}{d\omega d\Omega},$$

where  $I_L$  is the laser intensity (power per unit area);  $T_i$  and  $T_s$  are transmission coefficients at the sample-air interface for the incident and scattered photons, respectively;  $V$  is the effective scattering volume;  $\Omega_{\text{in}}$  is a solid angle inside the sample from which the scattered photons enter the collection optics (see Fig. 1);  $d^2\sigma/d\omega d\Omega$  is the Raman cross section per unit solid angle per unit volume per unit frequency shift, and  $\Delta\omega$  is the spectral band pass of the spectrometer.

The scattering volume depends on the absorption coefficients at the incident ( $\alpha_i$ ) and scattered ( $\alpha_s$ ) photon frequencies (which are proportional to the inverse of the penetration depth):

$$V \propto \int e^{-\alpha_i z} e^{-\alpha_s z} dz = \frac{1}{\alpha_i + \alpha_s}.$$

The optical penetration depth  $\lambda$  is on the order of 700 Å in the investigated materials. This is many orders of magnitude smaller than the laser spot diameter  $d$  ( $\sim 50 \mu\text{m}$ ), which is in turn much smaller than the focal length  $L$  of the collimating lens ( $\lambda \ll d \ll L$ ). In this case the scattering region can be treated as a point source very close to the surface of the sample. Then from Snell's law  $\Omega_{\text{in}} = \Omega_{\text{out}}/n^2$ , where  $n$  is the refractive index of the material.  $\Omega_{\text{out}}$  depends only on the  $f$ -number of the collimating lens (Fig. 1).

$T_i$ ,  $T_s$ ,  $V$ , and  $\Omega$  depend on the optical constants,

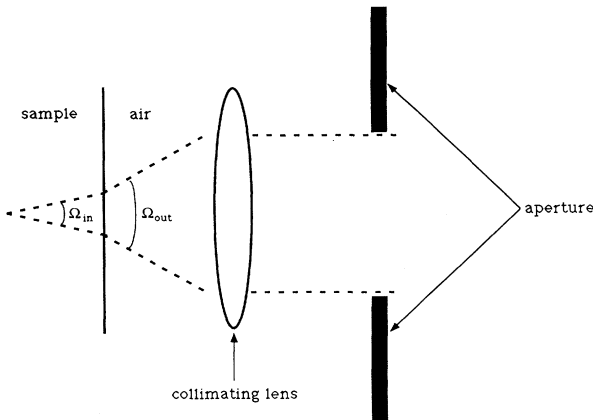


FIG. 1. Refraction of the scattered photons at the sample-air interface.

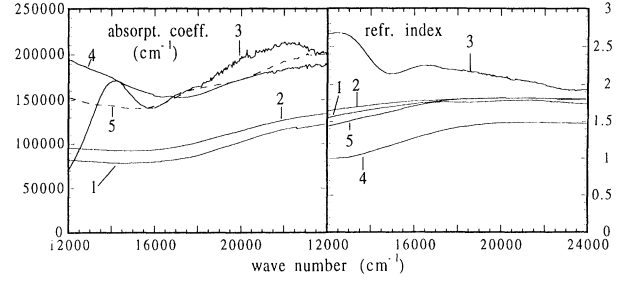


FIG. 2. Absorption coefficients (in  $\text{cm}^{-1}$ ) and refractive indices for the in-plane photon polarizations in (1)  $\text{YBa}_2\text{Cu}_3\text{O}_{6.6}$  ( $a$  axis), (2)  $\text{YBa}_2\text{Cu}_3\text{O}_{6.9}$  ( $a$  axis), (3)  $\text{YBa}_2\text{Cu}_3\text{O}_{6.1}$ , (4)  $\text{YBa}_2\text{Cu}_3\text{O}_{6.9}$  ( $b$  axis), (5)  $\text{YBa}_2\text{Cu}_3\text{O}_{6.6}$  ( $b$  axis).

which vary from material to material and need to be corrected for to make a comparison of the Raman cross sections in different materials meaningful. The spectra were multiplied by the sum of the absorption coefficients, square of the refractive index, and divided by the product of the transmission coefficients to correct for the optical absorption, transmission, and refraction:

$$\frac{d\sigma}{d\omega d\Omega} \propto \frac{P_s}{T_i T_s V \Omega_{\text{in}} I_L} \propto P_s (\alpha_i + \alpha_s) n^2 / (T_i T_s I_L). \quad (1)$$

The optical constants were obtained from polarized infrared (IR) reflectivity and ellipsometry measurements. The index of refraction and absorption coefficients of  $\text{YBa}_2\text{Cu}_3\text{O}_{6.1}$  (insulating phase),  $\text{YBa}_2\text{Cu}_3\text{O}_{6.6}$  ( $T_c = 66$  K), and  $\text{YBa}_2\text{Cu}_3\text{O}_{6.9}$  ( $T_c = 90$  K) at different in-plane photon polarizations are shown in Fig. 2, and the reflection coefficients are published in Ref. 5. The order of magnitude of these optical constants is the same at different polarizations and doping levels. The correction factor in Eq. (1) changes by less than  $\sim 30\%$  with doping for each polarization, and by less than  $\sim 60\%$  for different polarizations.

Intensity in all the spectra presented below is proportional to the energy cross section ( $d\sigma/d\omega$ ) per unit volume.

Raman spectra shown in Figs. 3(a), 4, and 8 were corrected for the optical constants; spectra shown in other figures were not corrected.

### III. DOPING DEPENDENCE OF THE TWO-MAGNON SCATTERING

Figure 3(a) shows spectra of an “as-grown” insulating single crystal  $\text{YBa}_2\text{Cu}_3\text{O}_{6.3}$ , an untwinned  $\text{YBa}_2\text{Cu}_3\text{O}_{6.6}$  single crystal ( $T_c = 66$  K), and an untwinned  $\text{YBa}_2\text{Cu}_3\text{O}_{6.9}$  single crystal ( $T_c = 90$  K). Doping dependence of the two-magnon scattering in twinned single crystals of  $\text{YBa}_2\text{Cu}_3\text{O}_{6.1}$ ,  $\text{YBa}_2\text{Cu}_3\text{O}_{6.3}$ ,  $\text{YBa}_2\text{Cu}_3\text{O}_{6.4}$  ( $T_c = 30$  K),  $\text{YBa}_2\text{Cu}_3\text{O}_{6.6}$  ( $T_c = 66$  K), and  $\text{YBa}_2\text{Cu}_3\text{O}_{6.9}$  ( $T_c = 90$  K) is shown in Fig. 3(b). Spectra in Fig. 3(b) were not corrected for optical constants, because the

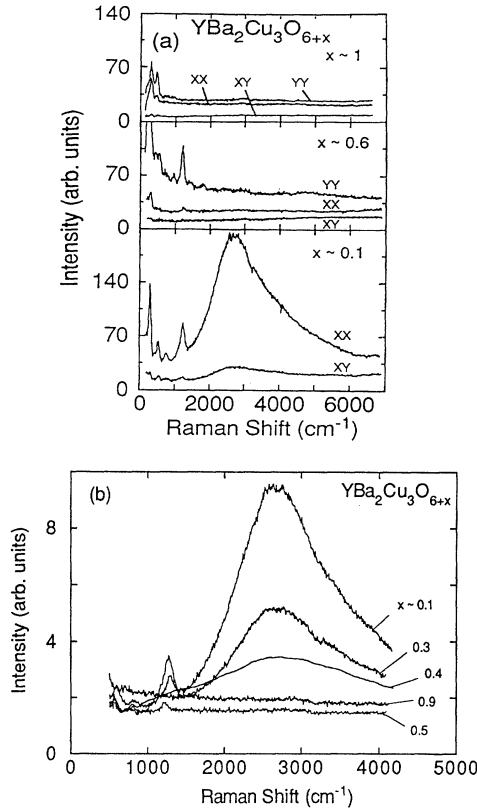


FIG. 3. (a) The continuum in untwinned  $\text{YBa}_2\text{Cu}_3\text{O}_{6.3}$  (insulating),  $\text{YBa}_2\text{Cu}_3\text{O}_{6.6}$  ( $T_c = 66$  K) and  $\text{YBa}_2\text{Cu}_3\text{O}_{6.9}$  ( $T_c = 90$  K) single crystals. Resolution  $\sim 50$   $\text{cm}^{-1}$ . (b) Doping dependence of two-magnon Raman scattering and the background continuum in twinned  $\text{YBa}_2\text{Cu}_3\text{O}_{6+x}$ . The spectra have not been corrected for the optical constants and the  $x \sim 0.4$  spectrum has been smoothed.

twinned crystals contain unknown ratios of  $X$  and  $Y$  oriented domains. The results have been confirmed on other samples.

In agreement with previous work<sup>6,7</sup> we observe a strong two-magnon scattering peak at  $\sim 2700$   $\text{cm}^{-1}$  in the insulating samples. The two-magnon scattering intensity decreases with doping and disappears completely in  $\text{YBa}_2\text{Cu}_3\text{O}_{6.6}$ .

#### IV. DOPING DEPENDENCE OF THE CONTINUUM AT 300 K

In addition to the two-magnon scattering, a strong background continuum extending above  $10000$   $\text{cm}^{-1}$  was also present in the insulating samples<sup>8</sup> (Figs. 3 and 4). The two-magnon scattering disappears with doping, but the continuum in  $XX$  geometry remains unchanged (Fig. 3).<sup>8</sup> The  $YY$  continuum is stronger than the  $XX$  continuum in the superconducting crystals. The  $X$ - $Y$  anisotropy is significantly greater in the oxygen deficient ( $T_c = 66$  K) sample than in the fully oxygenated ( $T_c = 90$  K) sample. Lower oxygen content of the  $\text{YBa}_2\text{Cu}_3\text{O}_{6.1}$  crystal than of the “as-grown”  $\text{YBa}_2\text{Cu}_3\text{O}_{6.3}$  crystal [Fig. 3(b)], resulted

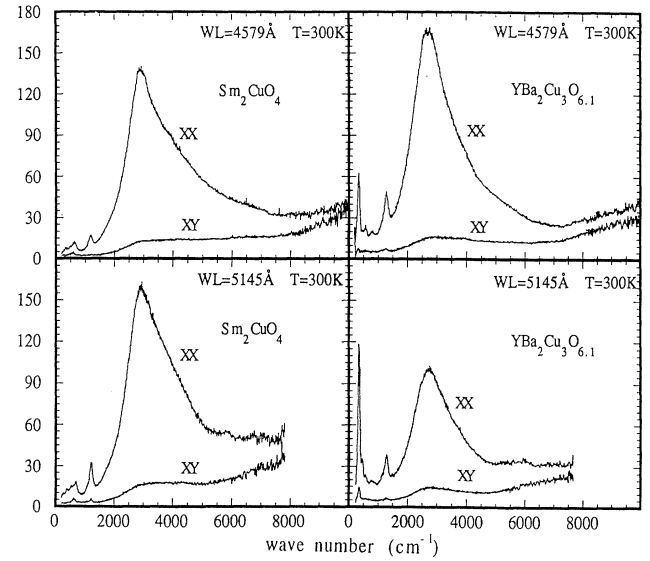


FIG. 4. The continuum and two-magnon scattering in  $\text{YBa}_2\text{Cu}_3\text{O}_{6.1}$  and  $\text{Sm}_2\text{CuO}_4$  at the incident laser wavelengths of  $4579$  and  $5145$   $\text{\AA}$ .

in a stronger two-magnon peak, but no change in the continuum.

Doping dependence of the continuum and the two-magnon peak similar to that reported above can be observed in the Raman spectra of 2:1:4 ( $R_2\text{CuO}_4$  family) and 1:2:3 ( $R\text{Ba}_2\text{Cu}_3\text{O}_{6+x}$  family) materials published by other groups.<sup>9–11</sup> However, one cannot extract information about the doping dependence of the continuum or two-magnon scattering intensities, because they did not correct their data for the doping dependent optical con-

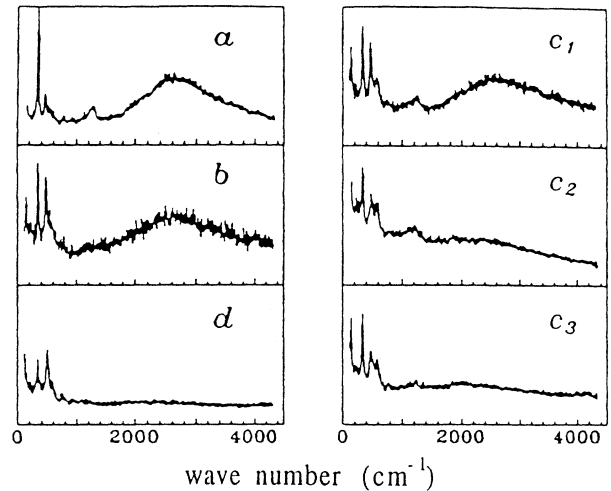


FIG. 5. The continuum and two-magnon scattering in  $\text{YBa}_2\text{Cu}_3\text{O}_{6+x}$  at different  $x$ . Room-temperature micro-Raman spectra were taken from (a) an undoped crystal and (b), (c), (d) different regions of an inhomogeneously doped crystal. Different strength of the two-magnon peak corresponds to different oxygen concentrations which varied between  $\sim 6.2$  and  $\sim 6.7$ .

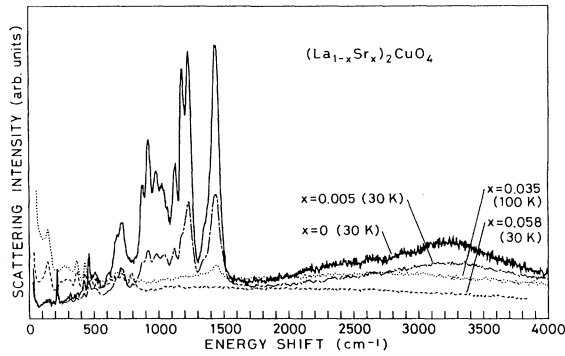


FIG. 6. The continuum and two-magnon scattering in  $(\text{La}_{1-x}\text{Sr}_x)_2\text{CuO}_4$  as a function of  $x$  (Ref. 10).

stants. In particular, the continuum in the insulating phases was overlooked, and it was often assumed that the two-magnon peak widens and eventually “redistributes” into the continuum.<sup>9</sup>

But because of a relatively small doping dependence of the optical constants in the relevant wavelength range (Fig. 2), Raman intensities change with doping roughly in the same way as the cross sections. It thus becomes meaningful to compare orders of magnitude of the intensities of the uncorrected spectra directly. Figure 5 shows another set of data on the doping dependence of plane-polarized 1:2:3 spectra,<sup>10</sup> Fig. 6 shows data of  $\text{La}_{2-x}\text{Sr}_x\text{CuO}_4$ ,<sup>9</sup> and Fig. 7 shows data of  $\text{Sm}_{2-x}\text{Ce}_x\text{CuO}_4$ .<sup>11</sup> These data confirm the result that the continuum cross section is roughly constant throughout the doping range. The two-magnon cross section decreases, as the doping is increased, disappearing entirely at high doping levels.

#### V. LASER WAVELENGTH DEPENDENCE OF THE CONTINUUM AND TWO-MAGNON SCATTERING IN $\text{YBa}_2\text{Cu}_3\text{O}_{6+x}$

The laser wavelength dependencies of the  $XX$  and  $YY$  continua of  $\text{YBa}_2\text{Cu}_3\text{O}_{6.9}$  at room temperature are shown in Fig. 8. The  $XX$  and  $YY$  continua are nearly flat at the

4579 Å incident laser wavelength and decrease with Raman shift at the longer laser wavelengths. The continuum intensity shows a weak enhancement towards the ultraviolet.

The two-magnon peak and the underlying continuum in  $\text{YBa}_2\text{Cu}_3\text{O}_{6.1}$  and  $\text{Sm}_2\text{CuO}_4$  at the 4579 and 5145 Å incident laser wavelengths are shown in Fig. 4. The two-magnon scattering intensity is roughly twice as strong at the 4579 Å wavelength in  $\text{YBa}_2\text{Cu}_3\text{O}_{6.1}$ , but the continuum is roughly unchanged.

The laser frequency dependence confirms the result on the resonant nature of the two-magnon scattering reported in Ref. 12. A detailed investigation of the laser frequency dependence as well as doping dependence of the two-magnon peak and the comparison to optical conductivity spectra shows that the peak can be observed only when the incident photons are at resonance with the charge-transfer gap feature observed in the conductivity. The disappearance of the two-magnon Raman peak upon doping occurs because the collapse of the charge-transfer gap destroys the coupling of the spin-flip excitations to the Raman process, not necessarily because of the disappearance of short-range antiferromagnetic order necessary to sustain two-magnon excitations.

#### VI. TEMPERATURE DEPENDENCE OF THE CONTINUUM

Although the continuum appears to weakly depend on doping at room temperature, temperature dependence below 1000  $\text{cm}^{-1}$  is different at different doping levels.

A comparison of the temperature dependence of the low-energy continuum in  $\text{YBa}_2\text{Cu}_3\text{O}_7$  and  $\text{YBa}_2\text{Cu}_3\text{O}_{6.1}$  single crystals was made in Ref. 13. It was shown that the continuum in  $\text{YBa}_2\text{Cu}_3\text{O}_7$  redistributes into a gaplike structure below  $T_c$ , which was not observed in the spectra of  $\text{YBa}_2\text{Cu}_3\text{O}_{6.1}$ . It was also concluded that in  $X'X'$  and  $X'Y'$  scattering geometries (as opposed to  $XX$ ) the continuum intensity at low energies was significantly stronger in  $\text{YBa}_2\text{Cu}_3\text{O}_7$  than in  $\text{YBa}_2\text{Cu}_3\text{O}_{6.1}$  if no corrections for optical constants are made. When these corrections (Sec. II C and Fig. 2) are taken into account, the  $X'X'$  and  $X'Y'$  continuum cross sections in

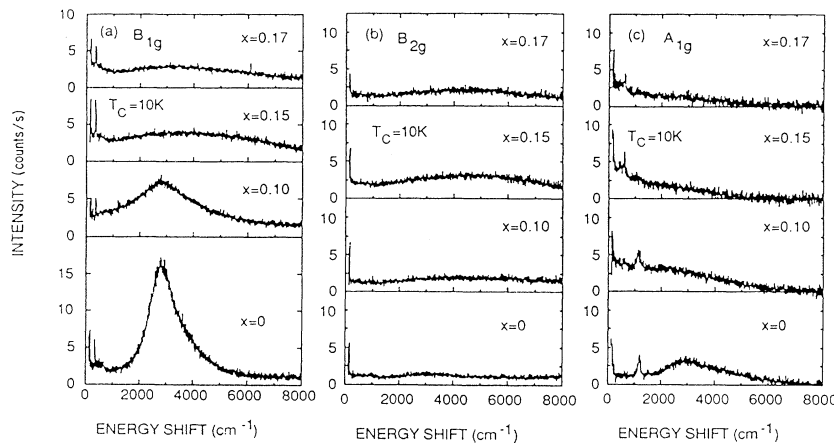


FIG. 7. The continuum and two-magnon scattering in  $\text{Sm}_{2-x}\text{Ce}_x\text{CuO}_{4-y}$  as a function of  $x$ . The scattering geometries are as follows.  $A_{1g}$ :  $X'X'$ , with  $XY$  spectrum subtracted out;  $B_{1g}$ :  $X'Y'$ ;  $B_{2g}$ :  $XY$  (Ref. 11).

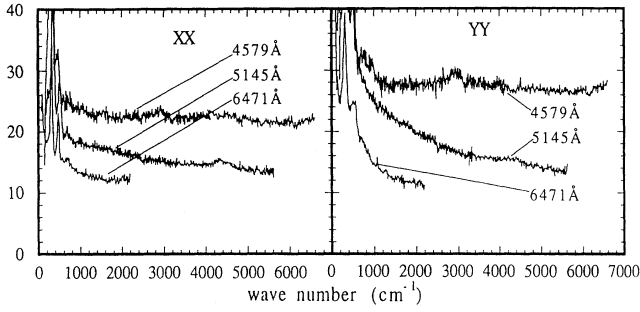


FIG. 8. Raman continuum in  $\text{YBa}_2\text{Cu}_3\text{O}_7$  in  $XX$  and  $YY$  geometry at different laser wavelengths.

$\text{YBa}_2\text{Cu}_3\text{O}_7$  are respectively a factor of  $\sim 2$  and  $\sim 1.5$  stronger than in  $\text{YBa}_2\text{Cu}_3\text{O}_{6.1}$ . The difference from the  $XX$  geometry might be due to a chain contribution.

This section presents the results on the temperature dependence of the Raman spectra of  $\text{YBa}_2\text{Cu}_3\text{O}_7$ ,  $\text{YBa}_2\text{Cu}_3\text{O}_{6.1}$ ,  $\text{YBa}_2\text{Cu}_3\text{O}_{6.35}$ , and  $\text{Sm}_2\text{CuO}_4$  in the frequency range of  $\sim 20$ – $800$   $\text{cm}^{-1}$ .

Though a number of studies on the temperature dependence of the continuum in  $\text{YBa}_2\text{Cu}_3\text{O}_7$  in the normal as well as in the superconducting state have been performed (for example, see Ref. 14), the results presented below have the best signal-to-noise ratios and most reliable laser heating estimates.

The temperature of the excited sample region ( $T_S$ ) is expected to be higher than that of the environment because of laser heating.  $T_S$  was determined from a comparison of the Stokes and anti-Stokes cross sections ( $\sigma_s$  and  $\sigma_{as}$ ), at the cryostat temperature  $T_0 = 60$  K from which it was extrapolated to other temperatures.

Figure 9 shows the spectrum of the  $\text{YBa}_2\text{Cu}_3\text{O}_{6.9}$  untwinned single crystal in the Stokes and anti-Stokes regions at  $T_0 = 60$  K.  $\sigma_s$  and  $\sigma_{as}$  are related by

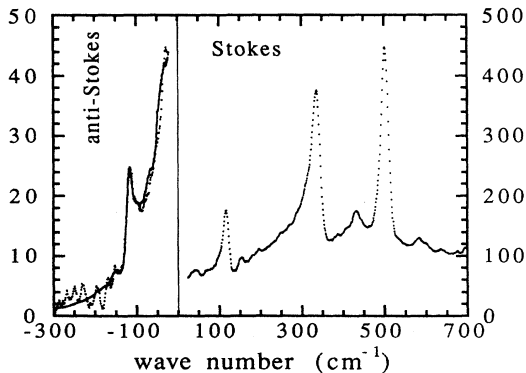


FIG. 9. The points represent the Raman scattering spectrum of  $\text{YBa}_2\text{Cu}_3\text{O}_{6.9}$  at the cryostat temperature of 60 K in the Stokes and anti-Stokes regions. Solid line in the anti-Stokes region is the Stokes experimental spectrum multiplied by a factor  $\exp(-\omega/T)$ , where  $T$  was equal 85 K. Note different scales for the Stokes (right) and anti-Stokes (left) spectra.

$$\frac{d^2\sigma_s}{d\omega d\Omega} = \frac{n_s^2 \omega_s^2}{n_L^2 \omega_L^2} e^{-\omega/k_b T} \frac{d^2\sigma_{as}}{d\omega d\Omega}.$$

We fit the anti-Stokes spectrum with the Stokes spectrum divided by  $\exp(-\omega/k_b T_S)$  using  $T_S$  as a parameter. The best fit to the anti-Stokes spectrum is obtained when  $T_S$  equals  $85 \pm 3$  K, thus implying the heating by about  $\sim 25$  K. This value is consistent with that reported in earlier work,<sup>15</sup> which showed that the laser heating of a few tens of degrees is expected even at rather small power densities due to the small thermal conductivity of the layered cuprates.  $T_S$  of the  $\text{YBa}_2\text{Cu}_3\text{O}_{6.1}$  crystal at  $T_0 = 60$  K calculated by the same method was  $90 \pm 3$  K.

It can be shown that  $\int_{T_0}^{T_S} \kappa(T) dT$ , where  $\kappa(T)$  is thermal conductivity, is independent of  $T_0$  and is proportional to the laser power density.<sup>15</sup> The integral was calculated using the value of  $T_S$  obtained from the Stokes–anti-Stokes ratio at  $T_0 = 60$  K.  $T_S$  for other  $T_0$  were estimated using the value of the integral, laser power density, and the functional form of the thermal conductivity of ceramic samples.<sup>16</sup> The error in Figs. 9–12, and 14 was  $\pm 7$  K, except for the 85 K (Figs. 9–12) and 90 K (Fig. 14) spectra where it was  $\pm 3$  K. The error in other figures was  $\pm 10$  K.

Energy scales affected by temperature are on the order of  $k_b T$  ( $\sim 200$   $\text{cm}^{-1}$  at 300 K); thus no temperature dependence of one-particle Raman spectra is expected above  $800$   $\text{cm}^{-1}$ . No temperature dependence of the continuum in  $\text{YBa}_2\text{Cu}_3\text{O}_{6.9}$  was observed above  $600$   $\text{cm}^{-1}$  at temperatures below 320 K.

Figure 10(a) clearly shows that within the experimental error the continuum does not depend on temperature in  $X'X'$  and  $XX$  geometries, even at the lowest energies, whereas the  $YY$  and  $X'Y'$  continuum intensities decrease with temperature at low energies. Phonon intensities scale with the Bose factor  $[1 + n(\omega, T)]$ .

Further insight can be gained by looking at the response functions. Imaginary parts of the Raman response function  $\text{Im}(R)$  obtained by dividing the spectra in Fig. 10(a) by the Bose factor  $[n(\omega, T) + 1]$  are shown in Fig. 10(b). The slope of the low-energy part of the continuum response function (below  $100$   $\text{cm}^{-1}$ ) increases with decreasing temperature in  $XX$  and  $X'X'$  geometries. The slope of the  $YY$  continuum response function increases slightly, but not as much as in  $XX$  and  $X'X'$  geometries. And, finally, the  $X'Y'$  response function shows no temperature dependence.

Figure 10(c) shows the ratios of the response functions at  $T = 320$ , 220, and 155 K to the response function at  $T = 110$  K. Smooth lines give the ratios expected from the marginal Fermi liquid (MFL) theory.<sup>17</sup> The agreement is good in  $XX$  and  $X'X'$  geometries. Deviations from the MFL behavior exist in  $YY$  and especially  $X'Y'$  geometries.

Thus, the current work does not confirm the MFL-like temperature dependence of the continuum in  $X'Y'$  geometry reported in Ref. 14. In agreement with Ref. 14 we do see the MFL-like temperature dependence in  $XX$  and  $X'X'$  geometries.

Temperature dependence of the continuum across the

superconducting transition is shown in Fig. 11(a). The continuum intensity decreases with temperature below  $T_c$  at low energies, and a broad peak appears between 350 and 550  $\text{cm}^{-1}$  in all scattering geometries. Such a redistribution of the continuum looks like the opening of the superconducting gap  $2\Delta$ , with the gap value of 400–500  $\text{cm}^{-1}$ . Dependence of this feature on the scattering geometry as well as the evidence for the gap anisotropy are discussed in detail in Ref. 13.

To separate the temperature dependence of the density of states from that due to the Bose factor, it is necessary to examine the response functions shown in Fig. 11(b). Although most temperature dependence of the spectra at low frequencies comes from the Bose factor, some depletion of the low-energy states occurs below  $T_c$ .

To obtain a more quantitative picture, we again look at the ratios of the response functions below  $T_c$  to the response function at  $T = 110$  K [Fig. 11(c)].

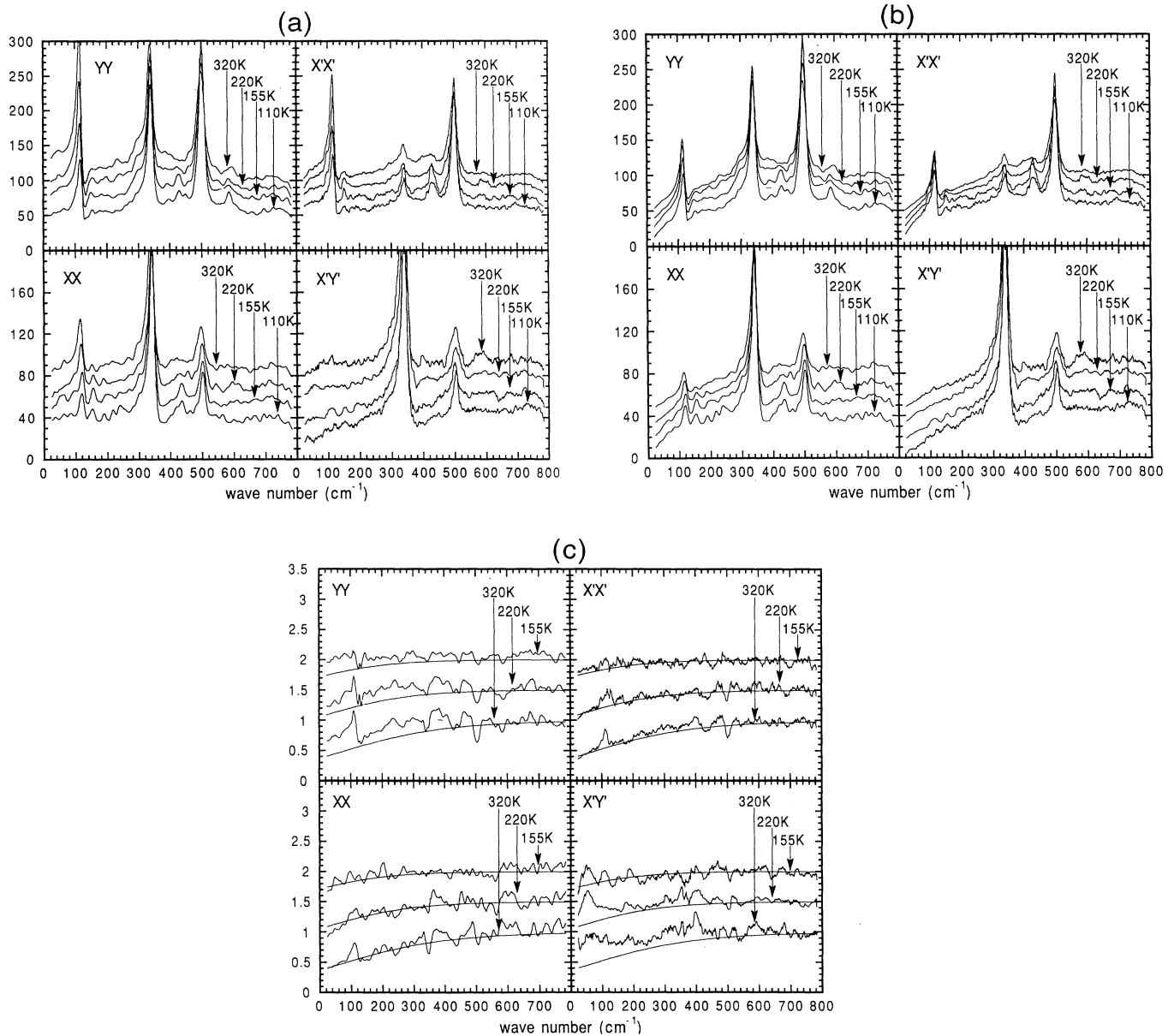


FIG. 10. (a) Temperature dependence of the Raman spectra of  $\text{YBa}_2\text{Cu}_3\text{O}_7$  above  $T_c$ . The 320, 220, and 155 K spectra were offset by 15, 30, and 45 units, respectively. (b) Temperature dependence of the imaginary part of the Raman response function of  $\text{YBa}_2\text{Cu}_3\text{O}_7$  above  $T_c$ . The 320, 220, and 155 K spectra were offset by 15, 30, and 45 units, respectively. (c) Ratios of the response functions at 320, 220, and 155 K to the response function at 110 K. The smooth lines represent the ratios expected from the marginal Fermi-liquid theory. The 320 and 220 K ratios were offset by 0.5 and 1, respectively.

The feature at  $330\text{ cm}^{-1}$  comes from the phonon anomaly. As the temperature drops through  $T_c$ , this phonon softens, broadens, and its integrated intensity increases by approximately a factor of 2 (Fig. 12). This result is discussed in detail in Ref. 18.

The broad peak between  $\sim 400$  and  $550\text{ cm}^{-1}$  comes from the gaplike redistribution of the continuum. This redistribution starts right below  $T_c$  (at  $T=85\text{ K}$ ), suggesting its relationship to superconductivity. According

to the BCS theory, the gap should be almost completely open at  $T \approx \frac{1}{2}T_c$ , which is the lowest temperature measured in our experiment. At this temperature, few states excited above the gap exist in the BCS picture, and the intensity at low energies could be due to “gapless” electrons. The fraction of the low-energy excitations that become “gapped” below  $T_c$  is equal to the ratio of the low-energy continuum response function at  $T \ll T_c$  to the response function above  $T_c$ . At  $40\text{ K}$  this fraction is

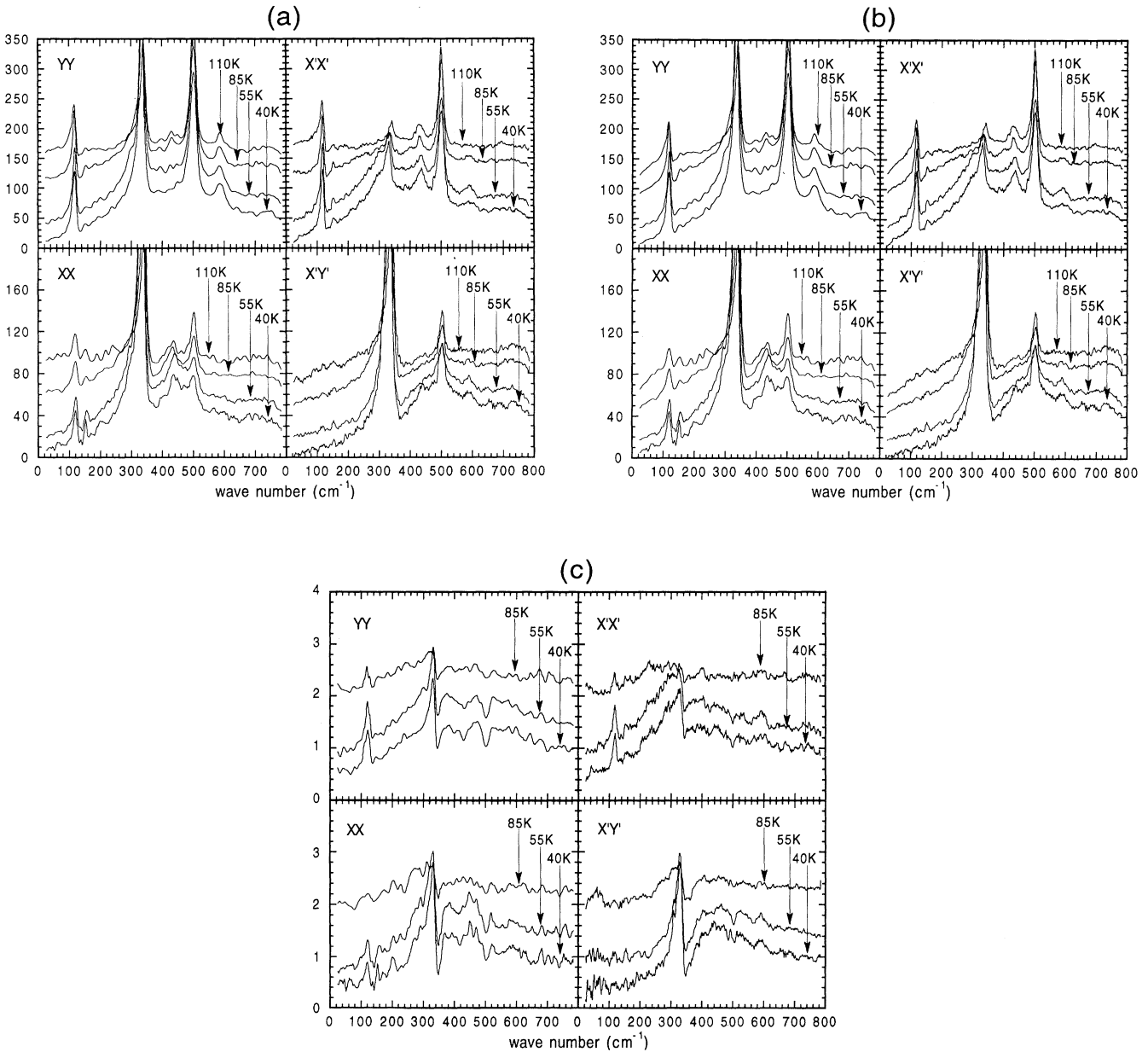


FIG. 11. (a) Temperature dependence of the Raman spectra of  $\text{YBa}_2\text{Cu}_3\text{O}_7$  across the superconducting transition. The 110, 85, and 55 K spectra were offset by 30, 90, and 120 units, respectively, in  $YY$  and  $X'X'$  geometries, and by 15, 45, and 60 units, respectively, in  $XX$  and  $X'Y'$  geometries. (b) Temperature dependence of the imaginary part of the Raman response function of  $\text{YBa}_2\text{Cu}_3\text{O}_7$  across the superconducting transition. The 110, 85, and 55 K spectra were offset by 30, 90, and 120 units, respectively, in  $YY$  and  $X'X'$  geometries, and by 15, 45, and 60 units, respectively, in  $XX$  and  $X'Y'$  geometries. (c) Ratios of the response functions at 40, 55, and 85 K to the response function at 110 K. The 55 and 85 K ratios were offset by 0.5 and 1.5, respectively.

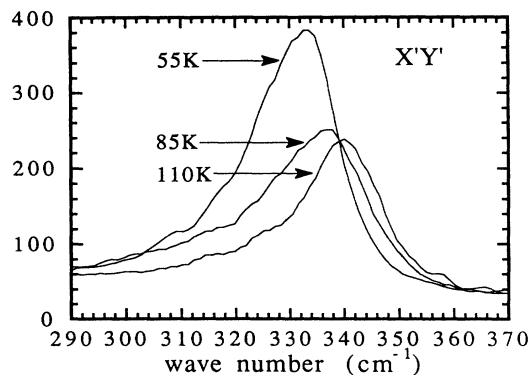


FIG. 12. The  $\sim 330 \text{ cm}^{-1}$  phonon in  $X'Y'$  geometry at 55, 85, and 110 K.

40–60 %, depending on the symmetry.

Temperature dependence of the continua in the insulating  $\text{YBa}_2\text{Cu}_3\text{O}_{6.1}$  [ $XX$ ,  $X'X'$ , and  $X'Y'$  geometries (Figs. 13 and 14)] and in  $\text{Sm}_2\text{CuO}_4$  [ $XX$  geometry (Fig. 15)] is different from that in the fully doped materials. The continuum intensity decreases with decreasing temperature throughout the region below  $800 \text{ cm}^{-1}$ . This is quite different from the temperature dependence given by the Bose factor. This temperature dependence can be fit fairly well, if the continuum in the undoped phases is assumed to be of two-Bose-factor character. In this case, to the first approximation, the cross section  $\sigma(T, \omega)$  is related to the cross section at zero temperature by<sup>19</sup>

$$\sigma(T, \omega) = \{n[T, (\omega/2)] + 1\}^2 \sigma(T=0, \omega).$$

Figure 16 shows the superimposed spectra of  $\text{Sm}_2\text{CuO}_4$  divided by the two-particle thermal factor  $\{n[T, (\omega/2)] + 1\}^2$ . Although the phonon lines do not match up (because phonons have single-Bose-factor tem-

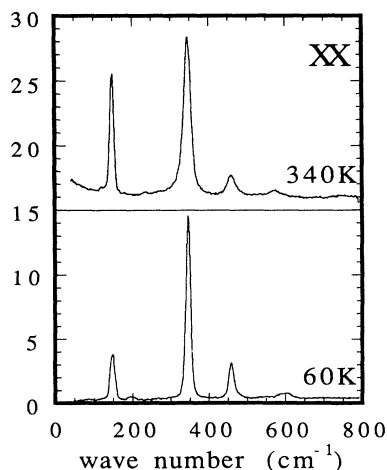


FIG. 13. Raman scattering spectra of  $\text{YBa}_2\text{Cu}_3\text{O}_{6.1}$  at 340 and 60 K in  $XX$  geometry.

perature dependence), the continuum scales with the two-particle thermal factor quite well. The results from  $\text{YBa}_2\text{Cu}_3\text{O}_{6.1}$  are similar.

Temperature dependence of the continuum becomes single-Bose-like once a small amount of doping is introduced, but before the metal-insulator transition is reached. Figure 17 shows the  $X'X'$  and  $X'Y'$  spectra of an insulating “as-grown” crystal with an approximate composition of  $\text{YBa}_2\text{Cu}_3\text{O}_{6.35}$  at  $T=60, 240,$  and  $340 \text{ K}$  divided by the Bose factor. Temperature independence of the resulting curves clearly shows that the continuum scales with the Bose factor, which is characteristic of scattering off of a single-Bose-like excitation.

In addition to the continuum and phonon modes allowed by symmetry, two dipole forbidden infrared-active modes<sup>20</sup> at  $\sim 210 \text{ cm}^{-1}$  and  $\sim 600 \text{ cm}^{-1}$  appear in the spectra of  $\text{YBa}_2\text{Cu}_3\text{O}_{6.1}$  and of  $\text{YBa}_2\text{Cu}_3\text{O}_{6.35}$  above 300 K in  $A_{1g}$  and  $B_{1g}$  symmetries. As the temperature is lowered below 240 K the  $210 \text{ cm}^{-1}$  mode disappears completely, and the  $600 \text{ cm}^{-1}$  mode decreases in intensity by an order of magnitude. Observations of the infrared active modes in  $\text{YBa}_2\text{Cu}_3\text{O}_{6.1}$  and in  $\text{YBa}_2\text{Cu}_3\text{O}_{6.35}$  at room temperature suggests the existence of a distortion of the unit cell that breaks the inversion symmetry above 300 K. As the temperature is lowered below 240 K, this distortion is greatly reduced, perhaps disappearing entirely.

The temperature dependence of the continuum in  $\text{YBa}_2\text{Cu}_3\text{O}_{6+x}$  can be summarized as follows: In undoped  $\text{YBa}_2\text{Cu}_3\text{O}_{6.1}$  the continuum scales with the two-boson thermal factor—the same is true for  $\text{Sm}_2\text{CuO}_4$ ; in the lightly doped but still insulating  $\text{YBa}_2\text{Cu}_3\text{O}_{6.35}$  the continuum scales with the usual Bose factor; in the fully doped superconducting  $\text{YBa}_2\text{Cu}_3\text{O}_7$  ( $T_c=90 \text{ K}$ ) above  $T_c$  the continuum scales with the Bose factor in  $X'Y'$  geometry. It is temperature independent in  $X'X'$  and  $XX$  geometries. In  $YY$  geometry the temperature dependence is somewhat smaller than that of the Bose factor. Below  $T_c$  a gaplike redistribution of the continuum occurs in all scattering geometries. The temperature dependence of the continuum in  $\text{YBa}_2\text{Cu}_3\text{O}_7$  reported above is also discussed in Ref. 13.

## VII. DISCUSSION

Strong evidence exists that the copper oxygen planes are responsible for the anomalous continuum in the Raman spectra of the layered cuprates. Properties such as its spectral shape, doping dependence, and temperature dependence are very similar in different materials. Moreover, it is not observed when the photons are polarized perpendicular to the planes. Assuming no defects in the planes, we might assign the Raman continuum to multiphonon processes,<sup>21</sup> spin-flip scattering,<sup>22</sup> intraband and interband electronic transitions,<sup>23</sup> or to acoustic plasmons expected to arise in layered materials.<sup>24</sup>

To understand constraints on the theoretical models of the continuum we consider the undoped phases first. The temperature dependence can be accounted for by two-boson scattering at low energies. Under the assumption of perfect crystal structures, we expect two types of exci-

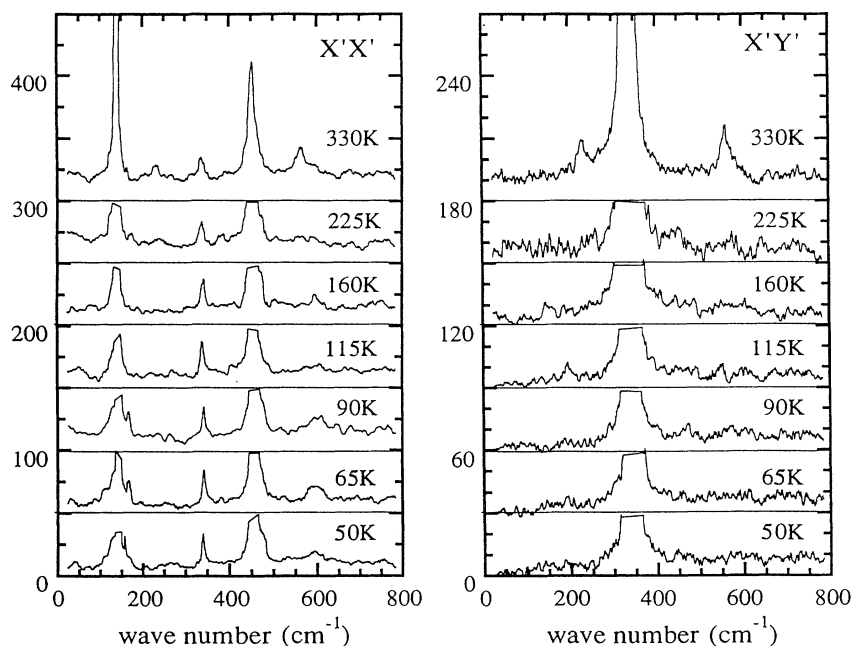


FIG. 14. Temperature dependence of the Raman continuum of  $\text{YBa}_2\text{Cu}_3\text{O}_{6.1}$  in  $X'X'$  and  $X'Y'$  geometries. Phonon lines were truncated.

tations below 1 eV: phonons and magnons. However, neither two-phonon nor two-magnon scattering can explain the experimental data.

Two-phonon (overtone) scattering intensity should be proportional to the two-boson thermal factor times the two-phonon density of states, which typically has sharp features. No two-phonon-like features are observed in the spectra. Another difficulty is the fact that the continuum extends up to  $10\,000\text{ cm}^{-1}$ , more than ten times greater than the phonon frequencies.

Two-magnon scattering, i.e., a low-frequency “tail” of the two-magnon peak is another possibility. This is supported by the fact that the continuum in the insulator is not observed in  $ZZ$  geometry, as expected from two-

magnon scattering. However, neither doping nor laser frequency dependence are consistent with this explanation. Two-magnon scattering does not account for the crossover to one-boson temperature dependence at small doping levels before the metal-insulator transition is reached. The laser wavelength dependence of the continuum in the undoped phases is completely different from that of the two-magnon peak and shows no evidence for the resonance with the charge-transfer excitation discussed in Sec. V and Ref. 12. In fact, a continuum in undoped  $\text{La}_2\text{CuO}_4$  is clearly seen above  $1000\text{ cm}^{-1}$  at a laser wavelength, at which no two-magnon scattering is observed (it is obscured by dense one and two-phonon lines at lower energies).<sup>25</sup>

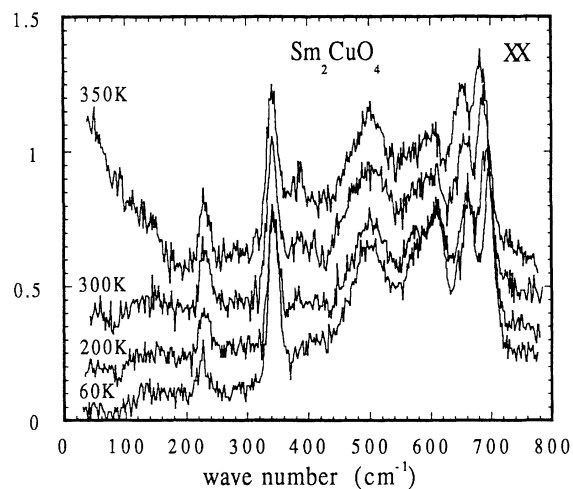


FIG. 15. Temperature dependence of the Raman scattering spectra of  $\text{Sm}_2\text{CuO}_4$  in  $XX$  geometry. The spectra were not offset.

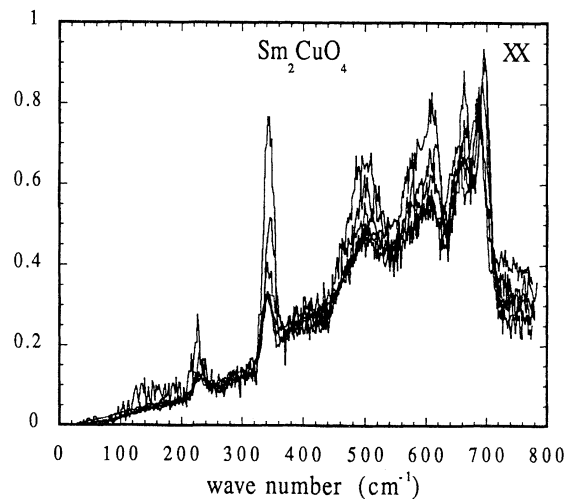


FIG. 16. Superimposed Raman spectra of  $\text{Sm}_2\text{CuO}_4$  divided by the two-particle thermal factor  $\{n[T,(\omega/2)]+1\}^2$  at the temperatures of 350, 300, 250, 200, 140, and 60 K.

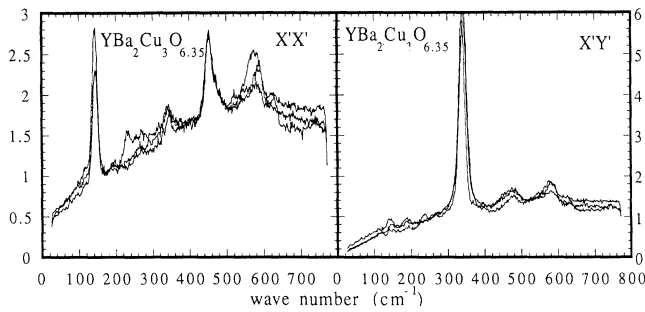


FIG. 17. Superimposed Raman spectra of  $\text{YBa}_2\text{Cu}_3\text{O}_{6.35}$  (lightly doped insulator) divided by the Bose factor  $[n(T, \omega) + 1]$  in  $X'X'$  and  $X'Y'$  geometries.

Thus, we have argued that perfect half-filled antiferromagnetic copper oxygen planes cannot produce the Raman continuum observed in the spectra of the undoped phases of the layered cuprates. Presence of the continuum implies an existence of localized electronic states, perhaps resulting from plane defects, impurities, or “extra” holes (or electrons) due to imperfect stoichiometry. Other evidence for the presence of localized states in the undoped phases comes from the spectra of  $\text{Im}(-1/\epsilon)$  (Ref. 26) derived from reflectivity measurements. Figure 18 shows that a broad continuum of states is present in  $\text{YBa}_2\text{Cu}_3\text{O}_{6.1}$  and  $\text{Sm}_2\text{CuO}_4$  below the charge-transfer gap,<sup>27</sup> which is supposed to be the lowest-energy optically active excitation for perfect half-filled copper oxygen planes.

Theories of the continuum in the doped phases must satisfy the following constraints imposed by experiment: (1) small doping dependence of the continuum intensity throughout the doping range in the 1:2:3 and 2:1:4 systems; (2) no anomaly across the metal-insulator transition; (3) two-particle-like temperature dependence in the “almost” undoped crystals; (4) crossover to a conventional one-particle temperature dependence in the lightly doped systems; (5) anomalous temperature dependence of

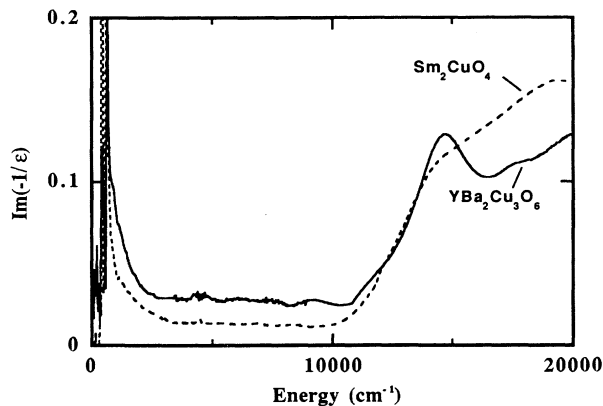


FIG. 18.  $\text{Im}(-1/\epsilon)$  derived from reflectivity measurements on  $\text{YBa}_2\text{Cu}_3\text{O}_{6.1}$  and  $\text{Sm}_2\text{CuO}_4$ . The onset above  $10000 \text{ cm}^{-1}$  is associated with the charge-transfer gap.

the continuum in the superconducting fully doped phases above  $T_c$ ; (6) an incomplete “gaplike” redistribution below  $T_c$ .

Persistence of the continuum into the insulating phase can exclude interband transitions (there are no interband excitations below 1.5 eV in the insulating phases) and plasmons.

Two types of theories of the continuum in the metallic phases are possible. Most existing theoretical models assume that the continuum in the metallic phases is a result of scattering by conduction electrons. An alternative approach is to assume that most of the continuum intensity comes from the excitation of localized states which result from holes (or electrons) trapped by structural imperfections, e.g., defects, impurities, or domain walls. (The latter case is discussed for the metallic phases by Phillips.<sup>28</sup>) In this case the role of conduction electrons would be limited to influencing the low-energy dynamics or contributing some intensity to the cross section directly at low energies.

Constraints the first condition places on the conduction electron model were discussed in detail in Ref. 8. There it was argued that the effective photon-continuum Raman coupling constant (the scattering vertex) must increase dramatically in magnitude with decreasing carrier concentration to cancel out the strong doping dependence of the number density of conduction electrons.

We consider three possible reasons for the conduction electron-photon coupling to increase in the metallic phases as the carrier concentration decreases.

(1) Photons couple to the effective charge density, which is screened for electron-hole excitations in the isotropic channel (i.e., screening reduces charge density associated with an electron-hole excitation). Screening is smaller for smaller carrier densities, so as the screening is decreased with decreased doping, the effective photon-electron coupling in the isotropic channel is expected to increase.

(2) Another possibility is an increase in Fermi surface anisotropy with decreasing carrier density. This would cause more scattering in the anisotropic channels (i.e., between different regions of the Fermi surface), which is not screened.

(3) Finally, it is reasonable to expect an increase in the electronic scattering rate with decreased doping, which would also tend to increase the scattering cross section.<sup>29</sup>

However, no theoretical arguments appeared to show that the doping dependence of the square of the photon-continuum coupling constant should scale closely with the inverse of the density of states of conduction electrons.

The density of defect induced localized states is in general (though not always) expected to depend on doping. This doping dependence cannot be understood without knowing the nature of these states. In the domain-wall model proposed by Phillips the density of localized states is expected to increase with doping, but at the same time their coupling to photons is expected to decrease.<sup>30</sup> Thus both models have to make similar assumptions to satisfy the constraint (1).

The absence of an anomaly at the metal-insulator tran-

sition [constraint (2)] automatically results from the localized-states picture (because conduction electrons do not have a strong effect on defects). It is unclear whether it would be possible to obtain the same result from the conduction-electron picture. One would have to show that, as the metallic material becomes an insulator, (a) the holes become localized in the antiferromagnetic environment, (b) their density never goes to zero due to imperfect sample stoichiometries, and (c) the mobility of these states does not have a strong effect on the Raman spectra.

To satisfy the constraints (3) and (4), both models have to assume that carrier-carrier interactions have a strong effect on the low-energy dynamics to produce the changes in the temperature dependence with doping.

In contrast, many theoretical models have been proposed to explain how electronic scattering can satisfy the constraint (5).<sup>16,31</sup> However, none of them predict the differences between different scattering geometries. It is unclear at this point whether the “localized states+conduction electrons at low energies” or the “conduction-electrons-only” model is better at explaining the observed temperature dependence of the continuum in the fully doped materials.

And, finally, the localized states picture has an explanation for the “gapless” states below  $T_c$ : Both conduction electron and localized states contribute to the continuum at low energies. The conduction electrons redistribute into a “gap” structure, and the localized states stay “in the gap” because they do not participate in superconductivity.

The conduction-electron picture must demonstrate that a large fraction of itinerant states does not become gapped at  $T \approx \frac{1}{2}T_c$  to satisfy the constraint (6). A non-zero-temperature calculation is necessary to find out if gap anisotropy resulting from anisotropic *s*- or *d*-wave pairing can account for all of the observed low-energy continuum intensity at 40 K. (The data show that approximately half the states which contribute to the continuum at low energies are gapless at 40 K.)

Thus, the conduction-electron picture does not provide a clear and unambiguous explanation for either of the experimental results discussed above. The localized-states picture automatically accounts for insensitivity of the integrated intensity of the continuum to doping and for a large fraction of “gapless” states below  $T_c$  and may be the better starting point for developing a microscopic theory of the Raman continuum in the cuprates.

## VIII. CONCLUSIONS

The plane-polarized continuum was found to be independent of doping in 2:1:4 and 1:2:3 materials at energies above  $\sim 1000 \text{ cm}^{-1}$ . Temperature dependence at low energies was found to differ significantly in the undoped, lightly doped, and fully doped  $\text{YBa}_2\text{Cu}_3\text{O}_{6+x}$ .

A feature consistent with the superconducting gap was observed below  $T_c$  in  $\text{YBa}_2\text{Cu}_3\text{O}_{6.9}$  in all scattering geometries. However, the “gaplike” redistribution was not complete, with 40–60% of states not shifted to higher energies at temperatures well below  $T_c$ .

Above  $T_c$  the temperature dependence strongly depends on the scattering geometry: the continuum is temperature independent (marginal-Fermi-liquid-like) in *XX* and *X'X'* geometry; it has a Bose-factor temperature dependence in *X'Y'* geometry, and a weak temperature dependence somewhat smaller than that of the Bose factor in *YY* geometry.

A two-boson-like temperature dependence of the low-energy continuum is found in  $\text{YBa}_2\text{Cu}_3\text{O}_{6.1}$  and  $\text{Sm}_2\text{CuO}_4$ . It becomes one-boson-like in YBCO once small doping levels are introduced.

Two alternative explanations of the continuum scattering in the copper oxide superconductors were examined: scattering by conduction electrons and scattering by localized states with a contribution from conduction electrons at low energies. Though neither model appeared to provide clear explanations of all the experimental results, predictions of the localized states picture appear to give the better agreement with the data.

## ACKNOWLEDGMENTS

D.R. would like to thank the Institute of Solid State Physics (Chernogolovka, Russia) for hospitality and partial support during his visit there. This work was supported by the NSF under Grant No. DMR 9017156 (D.R. and M.V.K.) and by NSF through the Science and Technology Center for Superconductivity under Grant No. DMR 912000 (S.L.C., M.V.K., W.C.L., and D.M.G.). A.A.M. and I.I.T. were supported in part by the NSF under a Soros Foundation Grant.

\*Present address: National Institute of Standards and Technology, Reactor Radiation Division, Bldg. 235/E151 Gaithersburg, MD 20899.

†Present address: McMaster University, Department of Physics and Astronomy, Hamilton, ON, Canada L8S 4M1.

<sup>1</sup>D. Reznik, A. L. Kotz, S. L. Cooper, M. V. Klein, W. C. Lee, and D. M. Ginsberg, in *Proceedings of the International Workshop on Electronic Properties and Mechanisms of High- $T_c$  Superconductivity* (IWEP), Tsukuba, Japan, 1991, edited by T. Oguchi, K. Kadowaki, and T. Sasaki (North-Holland, Amsterdam, 1992), pp. 283–287.

<sup>2</sup>S. L. Cooper, P. Nyhus, D. Reznik, M. V. Klein, W. C. Lee, D.

M. Ginsberg, B. W. Veal, A. P. Paulikas, and B. Dabrowski, *Phys. Rev. Lett.* **70**, 1533 (1993).

<sup>3</sup>J. P. Rice and D. M. Ginsberg, *J. Cryst. Growth* **109**, 432 (1991); W. C. Lee and D. M. Ginsberg, *Phys. Rev. B* **44**, 2815 (1991).

<sup>4</sup>G. H. Kwei, S.-W. Cheong, Z. Fisk, F. H. Garzon, J. A. Goldstone, and J. D. Thompson, *Phys. Rev. B* **40**, 9370 (1989).

<sup>5</sup>S. L. Cooper, A. L. Kotz, M. A. Karlow, M. V. Klein, W. C. Lee, J. Giapintzakis, and D. M. Ginsberg, *Phys. Rev. B* **45**, 2549 (1992).

<sup>6</sup>S. Sugai, Y. Entomoto, and T. Murakami, *Solid State Commun.* **72**, 1193 (1989).

- <sup>7</sup>K. B. Lyons, P. A. Fleury, R. R. Singh, and P. E. Sulewski, *Proc. SPIE* **1336**, 66 (1990); R. P. Singh, *Comments Cond. Matter Phys.* **15**, 241 (1991).
- <sup>8</sup>D. Reznik, M. V. Klein, W. C. Lee, D. M. Ginsberg, and S-W. Cheong, *Phys. Rev. B* **46**, 11 725 (1992).
- <sup>9</sup>S. Sugai, S. Shamoto, and M. Sato, *Phys. Rev. B* **38**, 6437 (1988).
- <sup>10</sup>A. V. Bazhenov, A. A. Maksimov, D. A. Pronin, I. I. Tartakovskii, and V. B. Timofeev, *Physica C* **169**, 381 (1990).
- <sup>11</sup>I. Tomeno, M. Yoshida, K. Ikeda, K. Tai, K. Takamuku, N. Koshizuka, S. Tanaka, K. Oka, and H. Unoki, *Phys. Rev. B* **43**, 3009 (1991).
- <sup>12</sup>S. L. Cooper, D. Reznik, A. Kotz, M. A. Karlow, R. Liu, M. V. Klein, W. C. Lee, J. Giapinzakis, and D. M. Ginsberg, *Phys. Rev. B* **47**, 8233 (1993); Ran Liu, S. L. Cooper, M. V. Klein, W. C. Lee, S-W. Cheong, and D. M. Ginsberg, *ibid.* **47**, 8233 (1993).
- <sup>13</sup>A. A. Maksimov, A. V. Puchkov, I. I. Tartakovskii, D. Reznik, M. V. Klein, W. C. Lee, and D. M. Ginsberg, *Pis'ma Zh. Eksp. Teor. Fiz.* **56**, 587 (1992) [*JETP Lett.* **56**, 570 (1992)].
- <sup>14</sup>F. Slakey, M. V. Klein, J. P. Rice, and D. M. Ginsberg, *Phys. Rev. B* **43**, 3764 (1991).
- <sup>15</sup>A. A. Maksimov, A. V. Puchkov, I. I. Tartakovskii, V. B. Timofeev, D. Reznik, and M. V. Klein, *Solid State Commun.* **81**, 407 (1992).
- <sup>16</sup>Yu. A. Kirichenko, K. V. Rusanov, and E. G. Tyurina, *Sverhprovodimost* **3**, 1076 (1990) [*Superconductivity* **3**, 1076 (1990)].
- <sup>17</sup>C. M. Varma, P. B. Littlewood, S. Schmidt-Rink, E. Abraham, and A. E. Ruckenstein, *Phys. Rev. Lett.* **63**, 1996 (1989).
- <sup>18</sup>R. Li, U. Weimer, R. Feile, C. Tome-Rosa, and H. Adrian, *Physica C* **175**, 89 (1991); C. Thomsen, in *Light Scattering in Solids VI*, edited by M. Cardona and G. Guntherodt (Springer, Berlin, 1991), Chap. 6.
- <sup>19</sup>M. V. Klein, in *Dynamical Properties of Solids*, Vol. 6, edited by G. K. Horton and A. A. Maradudin (Elsevier, New York, 1990), Chap. 2, pp. 65–127.
- <sup>20</sup>E. T. Heyen, J. Kircher, and M. Cardona, *Phys. Rev. B* **45**, 3037 (1992).
- <sup>21</sup>D. Mihailovic, K. F. McCarty, and D. S. Ginley, *Phys. Rev. B* **47**, 8910 (1993).
- <sup>22</sup>D. Pines (unpublished).
- <sup>23</sup>S. Rashkeev and G. Wendin, *Phys. Rev. B* **47**, 11 603 (1993).
- <sup>24</sup>V. Z. Kresin and H. Morawitz, *Phys. Rev. B* **37**, 7854 (1988).
- <sup>25</sup>M. Yoshida, S. Tajima, N. Koshizuka, S. Tanaka, S. Uchida, and T. Itoh, *Phys. Rev. B* **46**, 6505 (1992).
- <sup>26</sup>It can be shown that the Raman response function is equal to  $\text{Im}(-1/\epsilon)$ . For example, see J. M. Ziman, *Elements of Advanced Quantum Theory* (Cambridge University Press, Cambridge, 1969).
- <sup>27</sup>S. L. Cooper, W. C. Lee, D. M. Ginsberg, and S-W. Cheong (unpublished).
- <sup>28</sup>J. C. Phillips, *Phys. Rev. B* **41**, 8968 (1990).
- <sup>29</sup>M. Cardona and A. Zawadowski, *Phys. Rev. B* **42**, 10 732 (1990).
- <sup>30</sup>J. C. Phillips (private communication).
- <sup>31</sup>A. Virosztek and J. Ruvalds, *Phys. Rev. B* **45**, 347 (1992); P. W. Anderson, *Physica C* **185-189**, 11 (1991).